# THE PLASMA FOCUS AS A THRUSTER

A Thesis

by

RICHARD LEE HARDY

Submitted to the Office of Graduate Studies of
Texas A&M University
in partial fulfillment of the requirements for the degree of

MASTER OF SCIENCE

December 2004

Major Subject: Nuclear Engineering

# THE PLASMA FOCUS AS A THRUSTER

A Thesis

by

RICHARD LEE HARDY

Submitted to the Office of Graduate Studies of
Texas A&M University
in partial fulfillment of the requirements for the degree of

MASTER OF SCIENCE

Approved as to style and content by:

| | |
|---|---|
| _____ | _____ |
| Bruce Freeman<br>(Chair of Committee) | James Rock<br>(Member) |
| _____ | _____ |
| Wayne Saslow<br>(Member) | William Burchill<br>(Head of Department) |

December 2004

Major Subject: Nuclear Engineering

# ABSTRACT

The Plasma Focus as a Thruster. (December 2004)

Richard Lee Hardy, B.S., Texas A&M University

Chair of Advisory Committee: Dr. Bruce L. Freeman

The need for low propellant weight, high efficiency propulsion systems is a glaring need for various space missions. This thesis presents the thrust modeling of the Dense Plasma Focus plasma motion phases. It also contrasts some of the engineering tradeoffs between the existing coaxial plasma thrusters and the Dense Plasma Focus. Modeling the thrust generated by the DPF started with seeing how far the working models for the MPD would take the DPF. The effect of pulsed compared to quasi-steady state operation is computed. There is no known experimental data regarding thrust measurements for any DPF, so the thrust is analytically calculated using experimental data for the TAMU DPF. The calculated thrust is slightly higher than the thrust predicted by the models. The developed model shows that the force generated by the DPF will produce a thrust roughly three times the thrust for the MPD for similar input currents and electrode geometry. For the TAMUDPF to compete with the MPD as a thruster, it will need to be able to fire roughly 75 more times a second than the MPD.

TABLE OF CONTENTS

Page

ABSTRACT ..... iii

TABLE OF CONTENTS ..... iv

LIST OF TABLES ..... vi

LIST OF FIGURES ..... vii

CHAPTER

I INTRODUCTION ..... 1

Research Objectives ..... 2
Thesis Outline ..... 3

II THE DENSE PLASMA FOCUS ..... 4

Geometry ..... 4
Plasma Motion ..... 7
Inverse Pinch ..... 8
Rundown ..... 9
Collapse ..... 10
Pinch ..... 11
Propulsion ..... 14

III THE MAGNETOPLASMADYNAMIC THRUSTER ..... 16

Layout ..... 16
Thrust Models ..... 17
Erosion ..... 25

IV DPF PROPULSION ..... 26

DPF Thrust Phases ..... 26
Rundown ..... 26
Collapse ..... 29
Pinch ..... 33
Thrust Calculated from Working Data ..... 34
Duty Cycle ..... 38
Erosion ..... 39

CHAPTER Page

V CONCLUSIONS AND RECOMMENDATIONS ..... 42

REFERENCES ..... 44

VITA ..... 46

# LIST OF TABLES

TABLE Page

2.1 Thrust Results from Computer Modeling of the DPF ..... 15

4.1 Working Parameters for the TAMU DPF ..... 34

4.2 Dimensions and Max Current for TAMU DPF ..... 35

4.3 Calculated Forces and Velocities ..... 36

4.4 Actual TAMU DPF Forces, and Velocities ..... 36

4.5 Collapse Distance Effect on TAMU DPF Performance ..... 38

# LIST OF FIGURES

FIGURE Page

2.1 Plasma Focus Schematic ..... 5

2.2 TAMU DPF's Coaxial Electrodes and Insulator ..... 5

2.3 Stop Action Sequence of Inverse Pinch Phase ..... 8

2.4 Stop Action Sequence of Rundown Phase ..... 10

2.5 Stop Action Sequence of Collapse Phase ..... 11

2.6 Plasma Sheath Bouncing at the End of the Collapse Phase ..... 13

3.1 Layout of the MPD ..... 16

3.2 Jahn's Control Volume for MPD Derivations ..... 21

4.1 Position of Plasma Sheath Vertex During Collapse ..... 30

4.2 Plasma Sheath Approximation During the Collapse Phase ..... 31

4.3 Original End of the Anode Hole for TAMU DPF ..... 40

4.4 End of the Anode Erosion for the TAMU DPF ..... 41

# CHAPTER I

## INTRODUCTION

Plasma propulsions systems have been looked at for many years now as a possible way to travel in space. The primary advantage of plasma propulsion systems is the weight savings that is possible over a conventional chemical rocket. In modern terms, this weight savings translates into saving manpower, resources, and money. Plasma propulsion systems are still primarily in the research and development stage, with few plasma thrusters currently operational on space missions.

The Dense Plasma Focus (DPF) is a plasma machine whose main use over the last 50 years has been to make neutrons. Using its ability to obtain the temperatures and pressures necessary for fusion, the DPF produces neutrons when fuels such as deuterium and deuterium-tritium are used. In the past, researchers have considered the DPF for space propulsion missions, but little work has been done in this area. The DPF produces a plasma in the annular space between two coaxial electrodes when a capacitor bank is discharged into its fuel. The DPF operates in a strictly pulsed mode, meaning that the time of action is much smaller than the time between actions. Steady state is not reached during its operation. The DPF has potential as a thruster because the majority of the plasma motion and momentum occurs along the axis of the coaxial electrodes.

The Magnetoplasmadynamic Thruster (MPD) is a similar plasma machine to the DPF, and has been researched for the last 40 years. The MPD also uses coaxial

---

This thesis follows the style and format of the *Journal of Propulsion and Power*.

electrodes, but operates in a quasi-steady regime. By quasi-steady, it is meant that the forces on the plasma in the system exist long enough for the plasma to reach an equilibrium state. The MPD produces thrust by accelerating the plasma by way of the Hall Current, or $\vec{J} \times \vec{B}$ forces. These are the same forces that cause the plasma motion for the DPF. A plethora of thrust measurements exist for the MPD, along with well proven theoretical models. The theoretical models are based upon the coaxial geometry and a constant input current. The MPD is one of the highest thrust producing plasma machines in existence today.

The theoretical models developed for the MPD are geometry based; therefore, the thrust produced by certain phases of plasma motion for the DPF can be inferred by altering the MPD's initial conditions. New models will need to be developed for the thrust produced at the end of the center electrode for the DPF, because of characteristic differences between the MPD and the DPF.

## A. Research Objectives

The primary goal of the present research is to estimate the thrust produced by each relevant phase of plasma motion for the DPF and determine how well the MPD's models translate to similar geometries and different input currents. The secondary goal is to compare the thrust produced by the DPF to the MPD and begin a determination of the engineering tradeoffs between the two plasma machines. Ultimately, this will identify if the DPF is a viable option for space propulsion without fusion reactions, and whether or not the DPF should be studied further for propulsion applications.

To accomplish the objectives, theoretical models for the thrust produced by the DPF were developed. These models are extensions on the work done for the MPD, taking into account the differences between the two machines. A paper study was made to determine how engineering tradeoffs, such as erosion, influence the viability of the different coaxial plasma thrusters for space missions.

## B. Thesis Outline

This thesis consists of five chapters. The first chapter gives a brief introduction into plasma propulsion and sets out the goals for this thesis. The second chapter gives an in depth look at the DPF. It begins by covering the critical geometry of the DPF, the different phases of plasma motion and ends by giving a brief summary of the work with the DPF with regards to propulsion. Chapter III gives an overview of the MPD, and the relevant models for the various thrust phases. Chapter IV covers the thrust produced by the DPF. The models demonstrate how the DPF's input current and geometries affect the thrust produced. Next, the models developed to estimate the additional thrust terms for the DPF are derived. Then the specific impulse, efficiency, and experimental erosion are used to show the engineering tradeoffs between the coaxial thrusters. Chapter V concludes the thesis with conclusions and recommendations for future work.

# CHAPTER II

# THE DENSE PLASMA FOCUS

This chapter begins by introducing the geometry of the Dense Plasma Focus. It then proceeds with a description of each phase of motion for the DPF. The chapter then ends with the previous work on DPF propulsion.

## A. Geometry

The Dense Plasma Focus, or Plasma Focus, is a coaxial plasma gun with the center electrode having positive polarity. It consists of coaxial electrodes inside a vacuum system with an annular insulator running along the inner electrode. The insulator provides voltage standoff between the electrodes at the breach and provides initiation for the plasma sheath. Various machines, such as the Texas A&M University DPF (TAMU DPF), extend the outer electrode forming a back plate at the breach between the electrodes. This extension is so a knife edge can be formed along the insulator which helps improve the quality and uniformity of the plasma sheath that is created. A primary advantage of the coaxial geometry is the outer electrode counteracts the magnetic field produced by the center electrode, resulting in minimal magnetic field outside the electrode system. Figure 2.1 shows a simplified schematic of the plasma focus, and Figure 2.2 is a picture of the TAMU DPF. The length of the center electrode in Figure 2.2 is 30 cm. The axis labeled on Figure 2.1 will be used throughout the rest of this work.

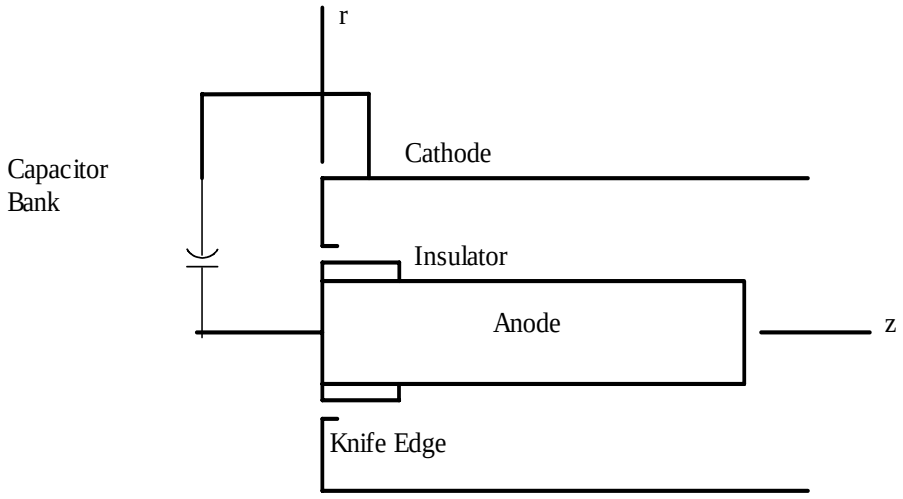


**Figure 2. 1 Plasma Focus Schematic**

**Figure 2.2 TAMU DPF's Coaxial Electrodes and Insulator**

The DPF operates in a snowplow mode. Initially, the desired fuel is placed into the vacuum system at very low pressures (torr range). The gas within the chamber will reach equilibrium before the DPF becomes operational. When the capacitor bank

attached to the electrodes is discharged, the gas will breakdown above the insulator forming a plasma. The plasma will then begin to move in a snowplow like motion. The plasma will form into a distinct sheath roughly a centimeter thick and will ionize the gas it encounters as it moves. The newly ionized gas will then be picked up by the plasma sheath and carried along through the rest of that phase of motion. Not all of the gas directly in front of the plasma sheath will be ionized and picked up by the sheath. Some of the gas will simply be pushed out of the way, or shed by the sheath. It is for these reasons that this type of plasma motion is referred to as a snowplow.

The capacitance storage acts as an Inductive/Capacitive (LC) circuit. The capacitor bank is in series with the two electrodes, with the plasma eventually completing the circuit between the two electrodes. The current discharge will produce a sine wave current, with the first quarter cycle being the rise time. This system does not act as a common LC circuit. As the plasma moves between the two electrodes, the circuit has a change of inductance because of the plasma physics involved. The voltage equation for this machine is shown in equation (2.1).

$$V = \dot{I}L + I\dot{L} + IR \tag{2.1}$$

Solving equation (2.1) for the different phases of motion is outside the scope of this thesis. Various assumptions are used instead of the solution to equation (2.1).

The anode is the inner electrode and is generally a right circular cylinder. The material typically used for the anode is copper. The anode can either be solid, or a pipe with thick enough walls to ensure that the magnetic field produced does not deform the shape of the anode. The diameter of the anode is chosen to optimize the plasma in the

later phases of the plasma motion. General sizes consist of a few centimeters in diameter for currents in the low kilo amp range to roughly ten centimeters in diameter for the mega amp range.

The cathode is the outer electrode. The original plasma focuses in the 1950's and 1960's used solid cylinder outer electrodes. A solid outer electrode is problematic because a portion of the gas is pushed out of the way by the moving plasma sheath and is collected at the cathode inner surface. The gas that is not ionized then moves toward the breach between the electrodes. When the gas reaches the breach, it will cause a new current sheath to form, more probably a spark. This hinders the performance of the DPF and led to the use of porous outer electrodes, which allowed the superfluous gas to escape. The porous outer electrodes eventually gave way to bar electrodes, which are currently used on mega ampere class machines.

The length of the anode determines how much fuel must be added to force the plasma sheath to reach the end of the anode at the quarter time of the capacitor bank. The cathode is normally as long, if not longer, than the anode. Since a connecting ring is used to support the outer electrode bars, on the TAMU DPF, the cathode is made longer to prevent the plasma sheath from attaching to the connecting ring during the collapse phase.

### B. Plasma Motion

The plasma focus has four distinct operating regimes: inverse pinch, rundown, collapse, and pinch. These phases consist of the plasma motion within the electrode system and the relevant phases for propulsion applications.

## 1. Inverse Pinch

The inverse pinch phase is the initial formation of the plasma sheath and its expansion from the insulator to the cathode. When the switch is initially closed, the gas will begin to breakdown above the insulator, forming a plasma between the knife edge of the cathode and the anode. The plasma sheath will begin to expand outward toward the cathode bars. This motion is typically referred to as an inverse pinch. The plasma sheath expands outwards with a snowplow action, increasing the amount of plasma in the sheath as it goes. The motion of this phase is primarily radial, with very little motion in the z direction toward the end of the anode. Approximately forty percent of the gas in this area remains in the plasma sheath at the start of the rundown phase. The inverse pinch for the TAMU DPF lasts roughly one microsecond. Figure 2.3 shows the stop action motion of the plasma sheath during the inverse pinch phase.

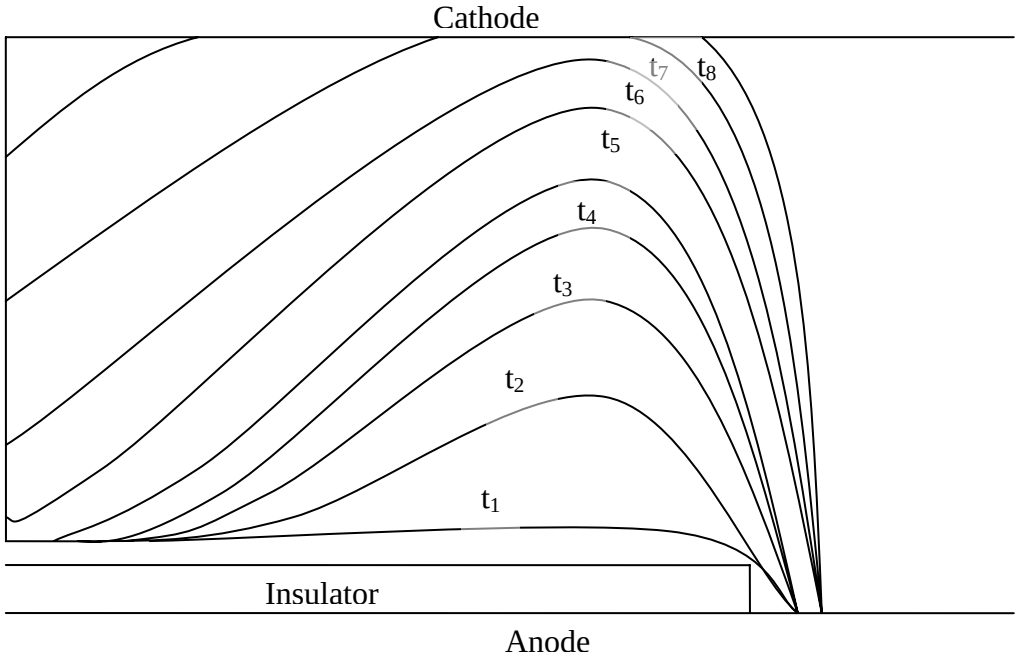


**Figure 2. 3 Stop Action Sequence of Inverse Pinch Phase**

## 2. Rundown

The rundown phase consists of the plasma sheath motion from the insulator to the end of the anode. In this phase, the plasma is accelerated by the $\vec{J} \times \vec{B}$ force, or Hall Current, toward the end of the anode. The magnetic field produced by the current flowing through the anode is strictly in the azimuthal direction which produces a force on the plasma in the z direction when the current flowing through the plasma is in the radial direction, hence the $\vec{J} \times \vec{B}$ force. It is this motion which results in these types of machines being called plasma guns. The plasma temperatures during the rundown phase range from 30-60eV. During this phase, the plasma motion acts as a snowplow. Due to the shape of the plasma sheath some of the ambient gas will be pushed out of the way through the electrode bars. Once the plasma moves outside the electrode bars, it is lost because there is minimal magnetic field outside a coaxial system. The plasma sheath is typically a few millimeters up to roughly a centimeter thick. The plasma sheath itself has an inner structure made up of current filaments. The rundown phase is timed along with the inverse pinch phase to force the plasma sheath to reach the end of the anode at the quarter time of the capacitor bank. This, in turn, causes the next two phases of plasma motion. Figure 2.4 shows the plasma motion during the rundown phase.

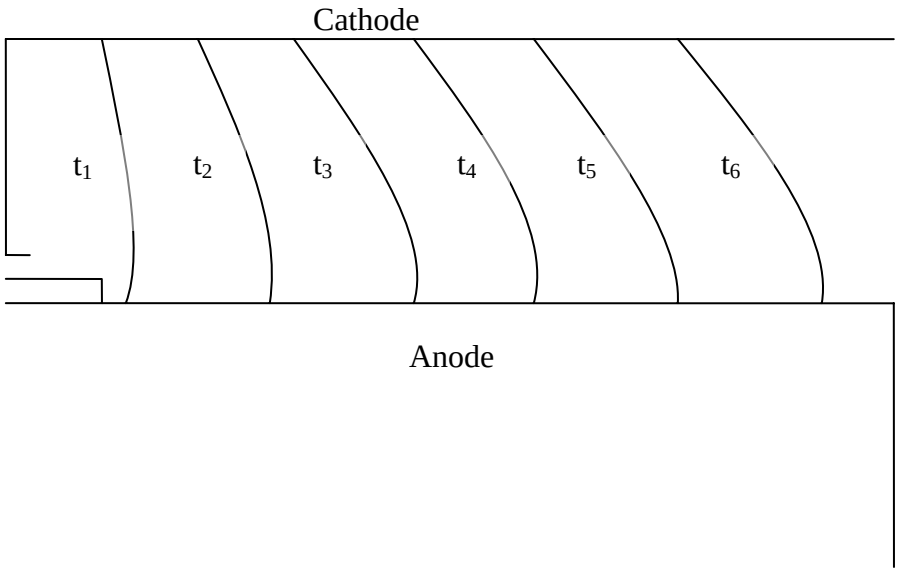


**Figure 2. 4 Stop Action Sequence of Rundown Phase**

### 3. Collapse

The collapse consists of what happens to the plasma sheath when it reaches the end of the anode. At the end of the rundown phase, the current and magnetic field will reach their maximum value. The large magnetic field causes the plasma sheath to collapse toward the electrode axis. During the collapse, an extension of the original plasma sheath grows in the region where the anode had been. The large magnetic field causes the sheath to move much faster in the negative radial direction than it does compared to its previous motion. The snowplowed ions from the rundown plasma sheath will continue on with roughly the same velocity and direction as they had at the end of the rundown. The ions in the sheath from the rundown will not turn the corner because there is no force acting on them to do so. To approximate what the sheath does, consider the sheath

in the collapse as an extension of the anode that will decrease in radius. The experimentally measured velocity of the plasma sheath in the collapse is approximately four times faster than the velocity of the sheath in the rundown. The plasma will end up with a parabolic shape extending up to the slower moving plasma exiting the rundown phase. The vertex of the parabola shaped plasma sheath is located roughly one half centimeter away from the end of the anode. The reasoning for this is that the pinch occurs one centimeter off the end of the anode. The time for the collapse for the TAMU DPF is on the order of 250 to 300 nanoseconds. Figure 2.5 shows an approximation of the plasma sheath shape in the collapse phase.

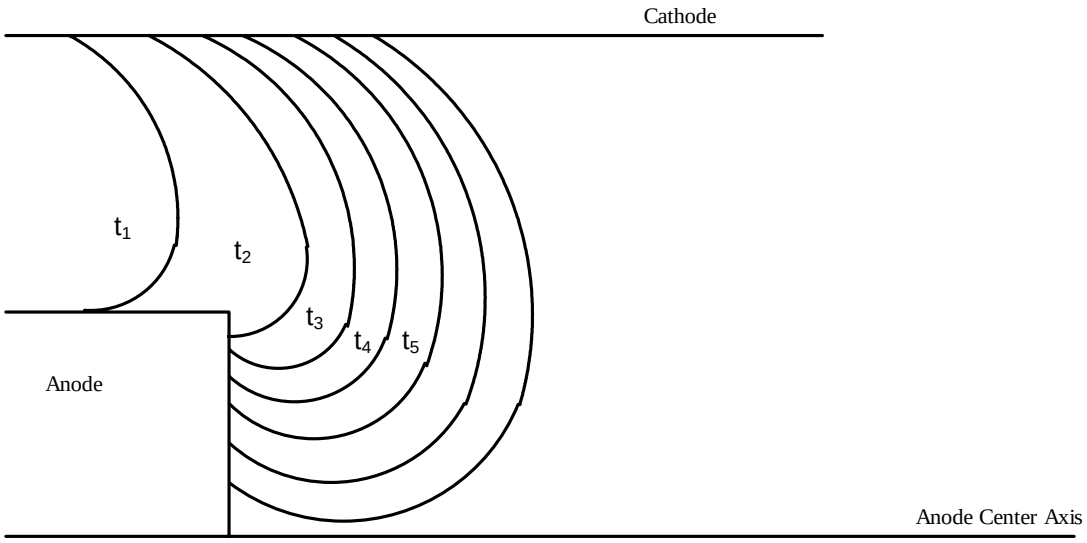


**Figure 2. 5 Stop Action Sequence of Collapse Phase**

## 4. Pinch

The pinch phase consists of the phenomenon that occurs when the plasma sheath reaches the electrode axis. As the plasma sheath collapses toward the electrode axis, the ambient gas is compressed. When the sheath reaches its furthest point of collapse it pinches the

gas that has a smaller radius than the sheath and accelerates the ions to very high velocities. The pinch is the location where fusion will occur.

The pinch takes place in the region off the end of the anode in the area less than the plasma sheath thickness above the plasma radius. The plasma radius is the closest point that the plasma in the collapse can reach. The standard approximation is that ten percent of the ambient gas from the collapse region is compressed within the plasma radius.

In the plasma snowplow model developed by Garwin and the Rosenbluth's[1], they solve the magnetohydrodynamic equations and show that the plasma sheath cannot reach the axis during the collapse phase. The physical reasoning behind this is that the pressure of the gas trapped in the pinch region increases as the plasma sheath reaches the axis that the pressure will slow the sheath and forces it to go the opposite direction. The plasma sheath will recoil until the driving magnetic field forces the sheath back inward because its force has overcame the pressure from the pinch region. This action is predicted in the snowplow model and is referred to as bouncing. Figure 2.6 shows the phenomena known as bouncing. The necking caused by the bouncing motion causes the plasma in the pinch region to circulate in the pinch region and even into the sheath itself. It is these circulating ions throughout the pinch that will collide causing fusion reactions when appropriate fuels are being used.

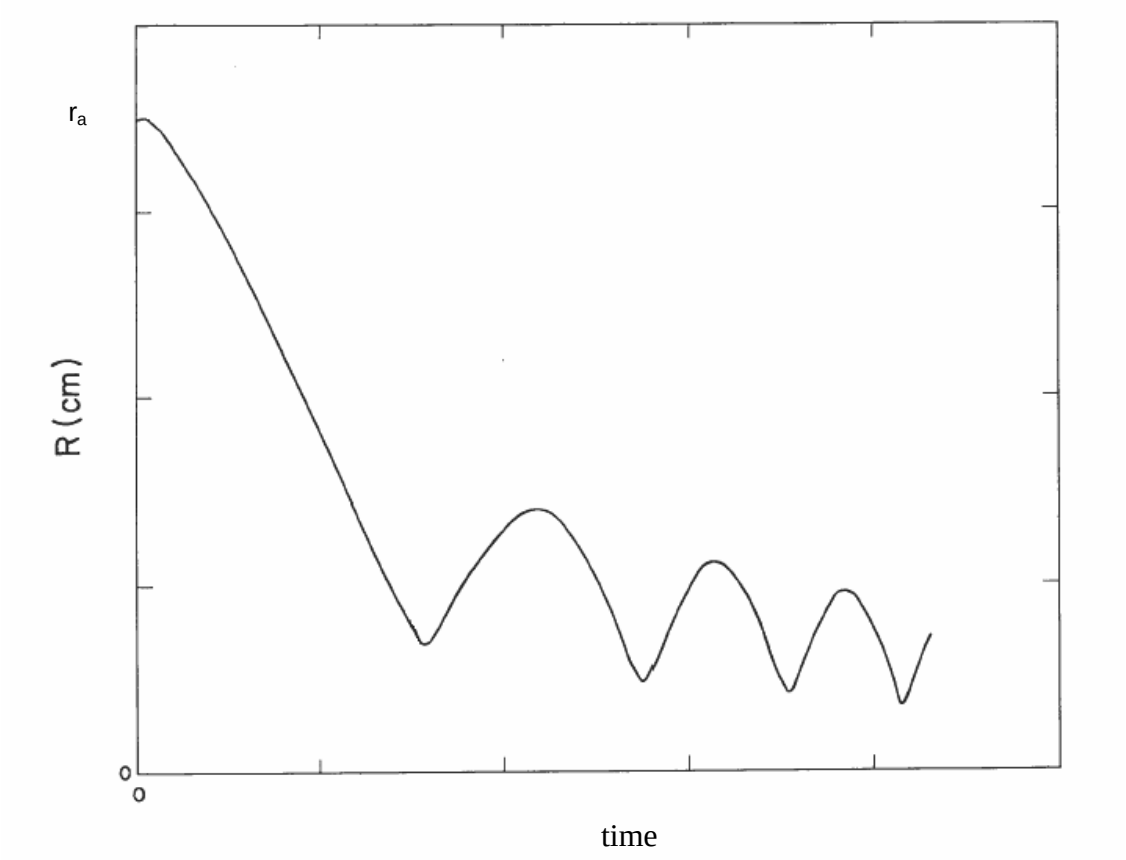


**Figure 2.6 Plasma Sheath Bouncing at the End of the Collapse Phase[1]**

Aside from the circulating motion, the plasma inside the sheath will experience a tremendous acceleration along the z-axis. Experimental measurements have shown that the low end ions out of the pinch have energies near 100 keV with the average energy being close to 400 keV, and the high energy tail going all the way up to 10 MeV. The energies just stated are for deuterium as a fuel and contain the extra energy that results from the fusion reactions. The impact fusion has on the ion distribution is unknown. As the plasma sheath collapses it has a parabolic shape which assists in channeling the plasma ions with a smaller radius than the sheath in the z-direction. The pinch region has dimensions of 1 cm in the z axis and roughly 1 mm in the radial direction. The pinch will

start about 1 cm off of the tip of the anode and move 1 cm in the z direction with an effect called zippering. The pinch lasts about one hundred nanoseconds.

## C. Propulsion

All known previous efforts for using the Dense Plasma Focus as a space thruster were conduct through the Air Force's Phillips Laboratory[2,3,4,5]. The goals of these efforts were to determine the thrust produced by the DPF using a computer code, test the necessary technology, and to measure the thrust experimentally.

Of all of three studies conducted, only one produced results with regards to the thrust produced by the DPF. Surprisingly, the one study that produced results did not result in a simple equation which estimates how thrust varies with respect to input currents and electrode spacing. The experimental and proof of concept work ended up having material problems that caused them not to be able to make experimental measurements.

The theoretical study was conducted by a group at Purdue University. For their theoretical study, they used a model based upon the tokamak-like m=0 instability. The tokamak is a donut shaped plasma fusion machine. This model is surprising because of the major differences between the governing plasma physics between the two machines. The results produced in this study are presented in Table 2.1. Their input parameters for these calculations were 20 MA for the pinch current and a propellant mass flow rate of 30 kg/s.

**Table 2.1 Thrust Results from Computer Modeling of the DPF**

| Parameter | Livermore-I DPF | EED DPF | Detailed Pinch DPF |
|---|---|---|---|
| Total Mass [kg] | 3.69E+05 | 3.59E+05 | 5.59E+05 |
| Total Thrust [N] | 4.73E+05 | 4.84E+05 | 9.07E+04 |
| Thrust-to-Weight | 0.131 | 0.137 | 0.0165 |
| Specific Impulse [s] | 1583 | 1607 | 973.6 |

The thrust is calculated using their computer code. Specific impulse is calculated using equation 2.2.

$$I_{sp} = \frac{F}{\dot{m}g} \tag{2.2}$$

Where force, F, is in Newtons, mass flow rate, $\dot{m}$, is in [kg/s], and g is gravity in mks units. Using the calculated specific impulse, thrust, and the electrical inputs, the efficiency, $E_{ff}$, of the thruster can be calculated using equation 2.3.

$$E_{ff} = \frac{\frac{1}{2}T \cdot I_{sp} \cdot g}{P} \tag{2.3}$$

The numerator of equation (2.3) also goes by the name of Jet Power. Power, P, is the energy divided by the time of operation. No data regarding the power was found in the Purdue effort, so the efficiency of the thruster according to their work remains unknown.

# CHAPTER III

# THE MAGNETOPLASMADYNAMIC THRUSTER

## A. Layout

The Magnetoplasmadynamic Thruster (MPD) is a coaxial plasma machine whose primary use has been propulsion for the last 40 years. The MPD is very similar to the DPF in geometry. The main differences between the MPD and DPF are polarity and how the current is inputted. Other differences consist of the placement of the insulator, the shape of the center electrode tip, and how the end of the outer electrode is shaped. The MPD is one of the highest thrust producing plasma machines.

The center electrode for the MPD is the cathode, with the outer electrode being the anode. The insulator is positioned along the inside surface of the anode. Usually the anode has a knob or ring at the end of insulator. Figure 3.1 depicts the layout of the MPD.

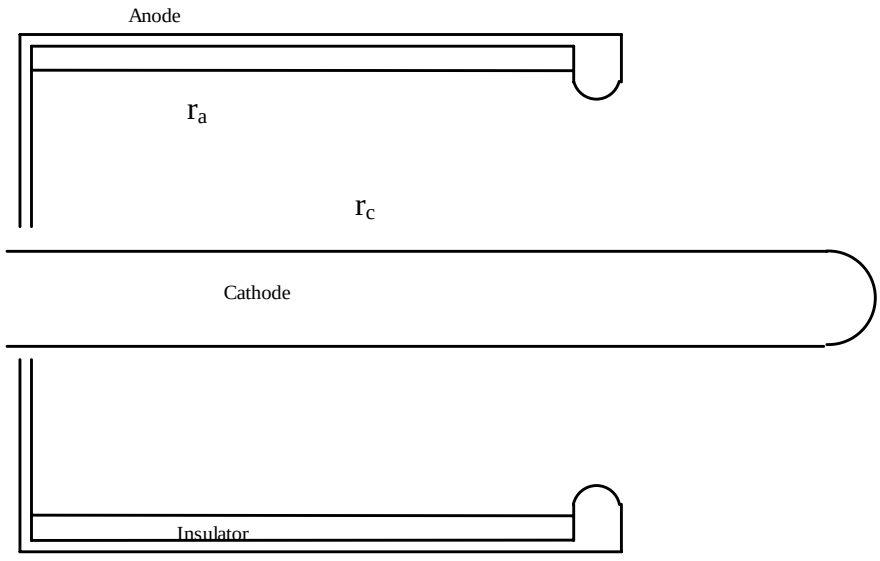


**Figure 3.1 Layout of the MPD.**

The cathode for the MPD is usually longer than the anode. The plasma formed by the MPD is not a distinct sheath. The MPD acts like an arcjet, whereas it creates a plasma that is the entire length of the cathode. The MPD operates with a quasi-constant current by using a ladder circuit system. The goal for the MPD is to be able to eventually operate completely as a steady state plasma thruster. The MPD operates with a gas puff mode. The gas puff mode consists of the vacuum system starting completely evacuated, and gas being puffed into the system using a fast action valve. When operating with a gas puff system, the MPD mass pulse lasts longer than the current pulse.

The thrust phases differ in title from the DPF because the MPD uses a diffuse discharge plasma. The backplate contribution is the thrust produced in the coaxial section of the MPD before the end of the cathode. The tip thrust term is the thrust produced by the hemispherical tip.

## B. Thrust Models

The first thrust model for the MPD was developed in the 1950's by Maecker[6]. This modeling determined the amount of thrust that would be produced by a coaxial plasma gun with constant input current. The most important result from this model is that it showed that thrust becomes appreciable for a coaxial system with input currents above 1 kA. When input currents above 1 kA are used, the thrust produced reaches the Newton level which is, to date, still higher than most plasma thrusters. Different modeling techniques were then applied by Jahn[7] and later Rudolph[8]. These improved the accuracy of the models.

The Maecker formula results from the solution of the Hall Current ( $\vec{J} \times \vec{B}$ ) and $\vec{\nabla} p$ (pressure) terms of the Magnetohydrodynamic (MHD) force equation. Equation (3.1) shows the simplified MHD force equation.

$$F = \int_V \vec{J} \times \vec{B} + \vec{\nabla} p \, dV \tag{3.1}$$

Where F is the force, $\vec{J}$ is the current density, $\vec{B}$ is the magnetic field, p is pressure and V is volume. Equation (3.2) shows the magnetic field dependence on a constant input and equation (3.3) shows the current distribution.

$$B_\theta = \frac{\mu J}{2\pi r}\left(1 - \frac{z}{z_0}\right) \tag{3.2}$$

$$J = 2\pi r z_0 j_r \tag{3.3}$$

Where $z_0$ is the length of the center electrode, r is the radius, z, is the variable distance along the center electrode, $j_r$ is the radial current density and J is the magnitude of the current density. For a coaxial geometry, equation (3.1) simplifies to the equation (3.4) excluding the pressure term.

$$f_z(r,z) = j_r B_\theta \tag{3.4}$$

The force is then found by solving equation (3.4), which steps are shown in equations (3.5), (3.6), and (3.7).

$$f_z(r,z) = j_r B_\theta = \frac{\mu_0 J^2}{4\pi r^2 z_0^{\,2}}\left(z_0 - z\right) \tag{3.5}$$

$$F_z = \frac{\mu_0 J^2}{4\pi z_0^{\,2}} \int_0^{z_0} \int_0^{2\pi} \int_{r_c}^{r_a} \frac{z_0 - z}{r^2} \, r \, dr d\theta dz \tag{3.6}$$

$$F_z = \frac{\mu_0 J^2}{4\pi} \ln\left(\frac{r_a}{r_c}\right) \tag{3.7}$$

The radius of the anode is $r_a$ and the radius of the cathode is $r_c$. Recall that the MPD uses a negative center electrode. The pressure distribution is calculated at the end of the cathode is computed by solving equation (3.8).

$$f_r = j_z B_\theta = \frac{\mu_0 J^2}{4\pi r_c^{\,2}} = -\frac{dp}{dr} \tag{3.8}$$

The pressure distribution used by Maecker is shown in equation (3.9).

$$p(r) = p_0 + \frac{\mu_0 J^2}{4\pi r_c^{\,2}}\left[1 - \left(\frac{r}{r_c}\right)^2\right] \tag{3.9}$$

Equation (3.10) shows the solution to equation (3.8).

$$F_c = 2\pi \int_0^{r_c} \left(p - p_0\right) r\,dr \tag{3.10}$$

Plugging equation (3.9) into equation (3.10) results in equation (3.11).

$$F = 2\pi \int_0^{r_c} \frac{\mu_0 J^2}{4\pi r_c^{\,2}}\left[1 - \left(\frac{r}{r_c}\right)^2\right] r\,dr \tag{3.11}$$

Equation (3.12) shows the force produced by the pressure term on the end of the cathode.

$$F = \frac{\mu J^2}{8\pi} \tag{3.12}$$

Jahn later expounded on Maecker's work. Jahn showed that the magnetic pressure dotted with the normal integrated over the area gives the same results. The use of the magnetic pressure allows for much more complicated geometries to be studied.

The magnetic pressure term comes from Maxwell's Equations. The short derivation for magnetic pressure follows:

The magnetohydrodynamic equation for force is given in equation (3.13).

$$\rho\frac{d\vec{v}}{dt} = \vec{J}\times\vec{B} - \vec{\nabla}p + \rho\vec{g} \tag{3.13}$$

The $\rho\vec{g}$ term is negligible. To determine the value of the $\vec{J}\times\vec{B}$ term, the Maxwell equations shown in equation (3.14) will be used.

$$\begin{aligned}\vec{\nabla}\times\vec{B} &= \mu_0\vec{J}\\ \vec{\nabla}\cdot\vec{B} &= 0\end{aligned} \tag{3.14}$$

$\vec{J}$ will be eliminated from these equations resulting in equation (3.15).

$$\vec{J}\times\vec{B} = \left(\vec{\nabla}\times\vec{B}\right)\times\frac{\vec{B}}{\mu_0} \tag{3.15}$$

$\left(\vec{\nabla}\times\vec{B}\right)\times\vec{B}$ can then be expanded as shown in equation (3.16).

$$\left(\vec{\nabla}\times\vec{B}\right)\times\vec{B} = \left(\vec{B}\cdot\vec{\nabla}\right)\vec{B} - \vec{\nabla}\left(\frac{B^2}{2}\right) = \vec{\nabla}\cdot\left(\vec{B}\vec{B}\right) - \vec{\nabla}\cdot\left(I\cdot\frac{B^2}{2}\right) \tag{3.16}$$

Equation (3.17) shows equation (3.16) in matrix form for cylindrical coordinates.

$$\mathrm{B} = \frac{1}{\mu_0}\begin{pmatrix} B_r^2 - \frac{B^2}{2} & \frac{B_rB_\theta}{r} & B_rB_z \\ \frac{B_\theta B_r}{r} & \frac{B_\theta{}^2 - \frac{B^2}{2}}{r^2} & \frac{B_\theta B_z}{r} \\ B_zB_r & \frac{B_zB_\theta}{r} & B_z{}^2 - \frac{B^2}{2} \end{pmatrix} \tag{3.17}$$

In the problems for the cylindrical geometry of the plasma machines, $B_r = B_z = 0$; so the magnetic pressure matrix then collapses to equation (3.18).

$$\mathrm{B} = \frac{1}{\mu_0}\begin{pmatrix} -\frac{B_\theta^{\,2}}{2} & 0 & 0 \\ 0 & \frac{B_\theta^{\,2}}{2r^2} & 0 \\ 0 & 0 & -\frac{B_\theta^{\,2}}{2} \end{pmatrix} \tag{3.18}$$

The force is found by integrating $B \cdot n$ over the area, where n is the normal in the direction of the desired force. Figure 3.2 shows the control volume used for MPD the thrust calculations.

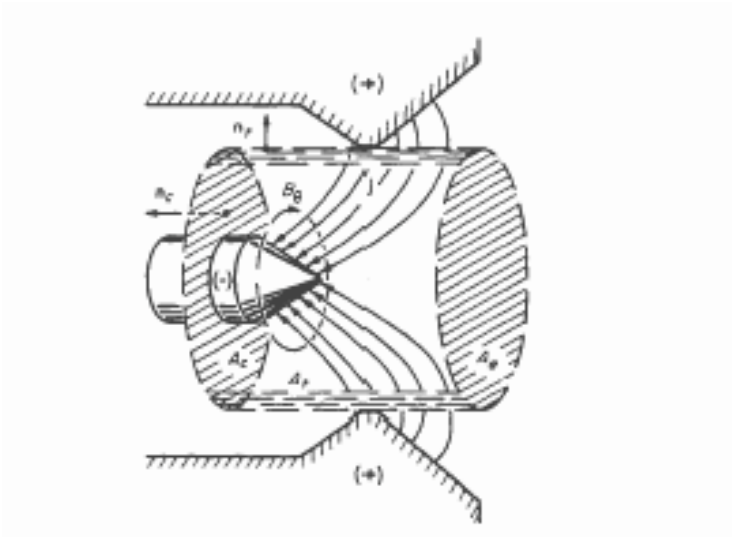


**Figure 3.2 Jahn's Control Volume for MPD Derivations[7]**

Using the control volume, Jahn was able to derive the thrust produced by the MPD using the following derivation. The magnetic field produced by the MPD or any cylinder of current is given in equation (3.19)

$$B_\theta = \begin{cases} \dfrac{\mu J}{2\pi r_c^2} r & r < r_c \\ \dfrac{\mu J}{2\pi r} & r > r_c \end{cases} \tag{3.19}$$

Then for the unit normal vector $n_c = 0, 0, -1$ the force in the z direction is given in equation (3.20).

$$\int_A \mathrm{B} \cdot n \, dA = \int_0^{r_c} \frac{B_\theta{}^2}{2\mu} 2\pi r \, dr \tag{3.20}$$

Solving equation (3.20) results in equation (3.21).

$$F = \frac{\mu_0 J^2}{4\pi} \left[ \ln\left( \frac{r_a}{r_c} \right) + \frac{1}{4} \right] \tag{3.21}$$

The pressure term adds the same result as produced by Maecker which is given in equation (3.12). So the total force produced by the MPD is shown in equation (3.22). Which is the same result produced by Maecker, just in a much more simplified derivation.

$$F = \frac{\mu_0 J^2}{4\pi} \left[ \ln\left( \frac{r_a}{r_c} \right) + \frac{3}{4} \right] \tag{3.22}$$

The Maecker formula was also improved by Rudolph. Rudolph took these equations one step further and found the force dependence on a hemispherical tip, losses to the outer electrode, and the effect of current dropping at the tip. Rudolph used the magnetic pressure approach to determine the thrust for the MPD. The simple derivation of the thrust produced by the hemispherical tip follows.

Equation (3.23) shows the current enclosed by the hemispherical tip.

$$J_{enc} = \int_0^r \frac{\varphi J}{A} dS \tag{3.23}$$

Where $\varphi$ is the fraction of total discharge current at the tip. The cathode tip differential area is then given by equation (3.24).

$$dS = 2\pi r \sqrt{\frac{r_c^{\,2}}{r_c^{\,2} - r^2}} dr \tag{3.24}$$

Substituting equation (3.24) into equation (3.23) results in equation (3.25).

$$J_{enc} = \frac{2\pi\varphi J}{A} \int_0^r r \sqrt{\frac{r_c^{\,2}}{r_c^{\,2} - r^2}} dr \tag{3.25}$$

Solving the integral in equation (3.25) results in equation (3.26).

$$J_{enc} = \frac{\varphi J}{A} 2\pi r_c \left( r_c - \sqrt{r_c^{\,2} - r^2} \right) \tag{3.26}$$

The magnetic field produced by the end of the cathode then becomes equation (3.27).

$$B_\theta = \frac{\mu_0 r_c \varphi J}{rA} \left( r_c - \sqrt{r_c^{\,2} - r^2} \right) \tag{3.27}$$

The magnetic pressure integral is then given by equation (3.28).

$$\int_S \left( \tilde{\beta} \cdot d\vec{S} \right)_{\substack{cathode \\ tip}} = \frac{\pi \mu_0 r_c^{\,2} \varphi^2 J^2}{A^2} \int_0^{r_c} \frac{\left( r_c - \sqrt{r_c^{\,2} - r^2} \right)^2}{r} dr \tag{3.28}$$

Solving equation (3.28) results in equation (3.29).

$$F = \frac{\mu_0 \varphi^2 J^2}{4\pi} \left[ \frac{3}{2} - 2\ln(2) \right] \tag{3.29}$$

The resulting pressure term from the hemispherical end follows a similar derivation. To find the pressure term, equation (3.13) is solved for the $\vec{\nabla} p$ term. Equation (3.30) then simplifies to equation accounting only for the radial component because the other terms will not contribute to the force in this geometry.

$$\rho u_r \frac{\partial u_r}{\partial r} = -\frac{\partial p}{\partial r} - j_z B_\theta \tag{3.30}$$

Solving equation (3.30) results in equation (3.31) which can then be solve and integrated over the area to determine the force produced by the pressure term.

$$p(r,z) = \int_r^{r_0} \rho u_r \frac{\partial u_r}{\partial r} dr + \int_r^{r_0} \frac{B_\theta}{\mu_0 r} \frac{\partial r B_\theta}{\partial r} dr + p(r_0, z) \tag{3.31}$$

$r_0$ is an arbitrary radius and $p(r_0,z)$ is the gasdynamic pressure at the arbitrary radius. The first integral is considered negligible because there is no known velocity radial dependence. Solving the second integral using equation (3.27) for the magnetic field and integrating over the tip area results in equation (3.32).

$$F = \frac{\mu_0}{4\pi} \frac{\varphi^2 J^2}{12} + p(r_c, z_{tip}) \pi r_c^{\,2} \tag{3.32}$$

The pressure term for the backplate contribution is given in equation (3.33).

$$F = p(r_a, z) \pi (r_a^{\,2} - r_c^{\,2}) \tag{3.33}$$

Rudolph's improvements also had terms that accounted for the outer electrode. These terms are not listed here because they of their dependence on experimental data, which is outside the scope of this thesis. So the total $\vec{J} \times \vec{B}$ force produced by the MPD is found by adding equations (3.7) and (3.29) together, with the pressure force resulting from the addition of equations (3.32) and (3.33).

## C. Erosion

Even though the MPD is one of the highest total thrust producing plasma thrusters, it is not heavily used. This is primarily due to an erosion problem that exists when the current reaches too high of a level. The level is called the onset current. The onset current is defined as the current at which the eroded particles surpass the amount of propellant in the plasma. This hampers performance because it reduces the effective lifetime of the thruster.

Onset current results from charge starvation of the outer electrode, when the current reaches too high of a level, or the propellant mass flow rate reaches too low of a level. When the current squared divided by the mass flow rate surpasses the onset current, the erosion of the outer electrode and insulator increases dramatically. This is also followed by massive voltage fluctuations. The onset current defines a maximum current and minimum mass flow rate that can be used by the MPD. The onset current prevents the MPD from scaling much higher than 40 kA, with less than 6 g/s mass flow rate of propellant.

# CHAPTER IV

# DPF PROPULSION

This chapter begins by determining how a sine wave input current will affect the thrust produced by a coaxial thruster. Then it derives the full set of thrust equations for the DPF. The thrust equations for the DPF are then compared to working experimental data for the TAMU DPF. Finally, a comparative analysis is made between the engineering tradeoffs between the MPD and the DPF.

## A. DPF Thrust Phases

The DPF will produce thrust during three of the four phases of plasma motion, rundown, collapse, and the pinch. The rundown force is modest in magnitude and will be very similar to the force derived for the similar phase of operation for the MPD. The collapse will have a larger force than the rundown phases, but not all of that force will be useful for propulsion applications. The pinch also produces a larger force than the rundown, with extremely high ion exit velocities resulting from the short time of the pinch.

### 1. Rundown

The time varying current case results in a time varying force. The first step to modeling the thrust produced by the DPF is to show how the different input current affects the total thrust produced during the rundown phase. With a sine wave as the input current, the current density J will be as stated in equation (4.1).

$$J = J_{\max} \sin\left(\frac{\pi}{2}\frac{t}{t_r}\right) \tag{4.1}$$

Where the $t_r$ is the rise time (quarter time) of the capacitor bank, t is the varying time, and the $\frac{\pi}{2}$ fraction is used to adjust the sine term to the correct values for the different fractions of the rise time. Since there is a varying time, the thrust will vary as the plasma sheath propagates in the rundown phase. Inserting equation (4.1) into the magnetic field equation results in equation (4.2).

$$B_\theta = \frac{\mu_0 J}{2\pi r} = \frac{\mu_0 J_{\max}}{2\pi r} \sin\left(\frac{\pi}{2}\frac{t}{t_r}\right) \tag{4.2}$$

Substituting equation (4.2) into the differential force equation results in equation.

$$F = \int_V j_r B_\theta dV = \frac{1}{(t_r - t_i)} \int_{t_i}^{t_r}\int_{r_a}^{r_c} \frac{\mu_0 J_{\max}^2}{4\pi r} \sin^2\left(\frac{\pi}{2}\frac{t}{t_r}\right) dr\, dt \tag{4.3}$$

$t_i$ is the initial current when the force begins to be applied. Integrating the radial dependence out of equation (4.3) and making the appropriate trigonometric substitution results in equation (4.4).

$$F = \frac{\mu_0 J_{\max}{}^2}{4\pi (t_r - t_i)} \frac{1}{2} \int_{t_i}^{t_r} 1 - \cos\left(\pi \frac{t}{t_r}\right) dt \tag{4.4}$$

Solving equation (4.4) results in equation (4.5).

$$F = \frac{\mu_0 J_{\max}{}^2}{8\pi (t_r - t_i)} \left[ (t_r - t_i) - \frac{t_r}{\pi} \sin\left(\pi \frac{t}{t_r}\right)_{t_i}^{t_r} \right] \tag{4.5}$$

Evaluating equation (4.5) at the limits of integration results in equation (4.6).

$$F = \frac{\mu_0 J_{\max}{}^2}{8\pi (t_r - t_i)} \left[ (t_r - t_i) - \frac{t_r}{\pi} \sin\left(\pi \frac{t_i}{t_r}\right) \right] \tag{4.6}$$

Equation (4.6) is the result of averaging the force produced over the time the force is produced, and is the $\vec{J} \times \vec{B}$ rundown term for the DPF.

The pressure term during the rundown phase turns out to be negligible. The differential pressure equation is given in equation (4.7).

$$\rho u_r \frac{du_r}{dr} = -\frac{dp}{dr} - j_z B_\theta \tag{4.7}$$

The solution of equation (4.7) is equation (4.8).

$$p(r,z) = \int_r^{r_0} \rho u_r \frac{\partial u_r}{\partial r} dr + \int_r^{r_0} \frac{B_\theta}{\mu_0 r} \frac{\partial (r B_\theta)}{\partial r} dr + p(r_0, z) \tag{4.8}$$

$r_0$ is an arbitrary radius and $p(r_0,z)$ is the gasdynamic pressure at the arbitrary radius. The second integral of equation (4.8) is zero because of the radial dependence of the magnetic field. The radial velocity term is an unknown and will be assumed to be slowly varying in the radial direction, making this term negligible as was done by Rudolph for the MPD. So the resulting force from the pressure during the rundown is shown in equation (4.9).

$$F = p(r_0, z)\pi(r_c^{\,2} - r_a^{\,2}) \tag{4.9}$$

The MPD uses experimentally measured pressure at their backplate to determine the gasdynamic pressure. Knowledge of the plasma sheath motion will be used for an initial estimate of the pressure force for the DPF. The pressure that is applied in the negative z direction after the plasma sheath starts to move results from the pressure or the gas that is left behind the sheath. As the plasma sheath snowplows between the two electrodes, it ionizes all of the atoms that are in its path. This implies that a vacuum is

left behind the sheath which is slightly incorrect. The sheath will leave behind some atoms that undergo recombination. For the DPF, the pressure of the gas behind the sheath compared to that in front of the sheath is approximated between 1/100 and 1/1000. For an initial fill pressure of ten torr, which is typical for the TAMU DPF with deuterium as a fuel, the pressure behind the sheath is less than one tenth of a torr. The pressure applied over the area between the electrodes at the breach results in a force less than two tenths of a Newton. This force is negligible compared to the other forces present.

**2. Collapse**

The forces during the collapse phase exist primarily in the negative radial direction. An approximation of the plasma sheath motion is that the vertex of the plasma sheath collapses to a distance $r_p$ above the electrode axis, while traveling only 0.5 centimeters in the z direction. The distance $r_p$ is the plasma radius, which is the distance of closest approach for the plasma sheaths to the axis. The current during the collapse phase, $J_c$, is assumed to be eighty percent of the maximum current and remain constant throughout the collapse phase. The current is approximated as constant because of the short amount of time needed for the collapse. Figure 4.1 shows a sketch approximating the position of the vertex of the sheath during the collapse.

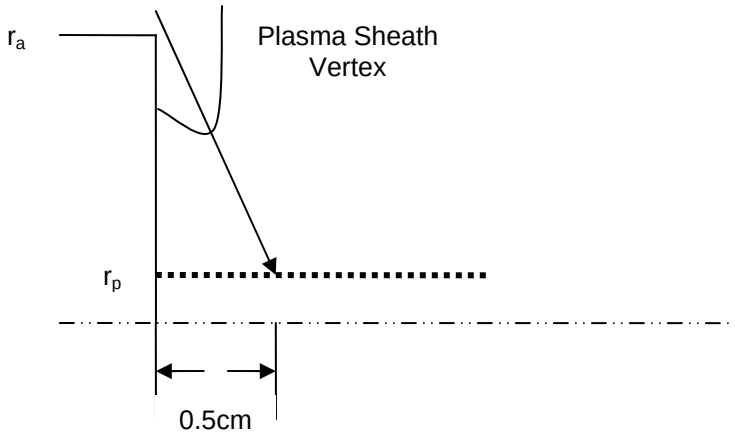


**Figure 4.1 Position of Plasma Sheath Vertex During Collapse**

During the rundown phase, the ideal plasma sheath for a thruster is strictly in the radial direction. During the collapse, a portion of the sheath will act like an extension of the anode that has a varying radius. This extension causes the same magnetic field dependence as the rundown phase. To approximate the collapse for modeling, it will be assumed that the plasma sheath will form a right angle during the collapse. This means that part of the sheath will act like an extension of the anode, with the rest being strictly in the radial direction. Figure 4.2 shows the sheath approximation during the collapse.

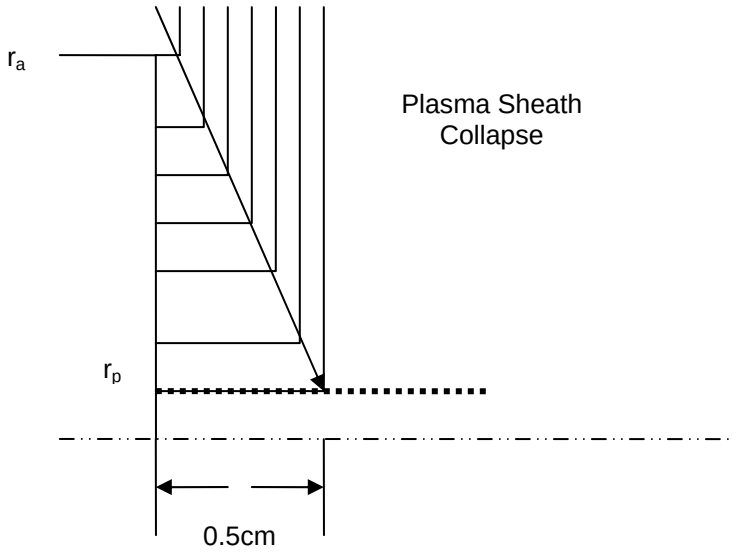


**Figure 4.2 Plasma Sheath Approximation During the Collapse Phase**

The magnetic field that would be now be driving the plasma sheath is given in equation (4.10).

$$B_\theta = \frac{\mu_0 J_c}{2\pi r} \quad r_p < r < r_a \tag{4.10}$$

$J_c$ is the current during the collapse phase. Equation (4.10) is the magnetic field produced outside a cylinder. To use the magnetic pressure approach to obtain the force, the radius will need to be changing from the variable radius $\alpha$ to the radius of the anode $r_a$. The force integral is shown in equation (4.11).

$$F = \int_{\alpha}^{r_a} \frac{1}{2\mu_0}\left(\frac{\mu_0 J_c}{2\pi r}\right)^2 2\pi r\, dr \tag{4.11}$$

$\alpha$ is the variable radius during the plasma sheath collapse. To produce useful results, equation (4.11) is averaged over the range of the collapse. The average force integral is shown in equation (4.12).

$$F = \frac{\mu_0 J_c^{\,2}}{4\pi} \frac{1}{\left(r_a - r_p\right)} \int_{r_p}^{r_a} \int_{\alpha}^{r_a} \frac{1}{r} dr d\alpha \tag{4.12}$$

Solving the first integral in equation (4.12) results in equation

$$F = \frac{\mu_0 J_c^{\,2}}{4\pi} \frac{1}{\left(r_a - r_p\right)} \int_{r_p}^{r_a} \left(\ln\left(r_a\right) - \ln\left(\alpha\right)\right) d\alpha \tag{4.13}$$

Integrating equation (4.13) results in equation (4.14) which then simplifies to equation (4.15).

$$F = \frac{\mu_0 J_c^{\,2}}{4\pi} \frac{1}{\left(r_a - r_p\right)} \left[ r_a \ln\left(r_a\right) - r_a \ln\left(r_a\right) + r_a - r_p \ln\left(r_a\right) - r_p \ln\left(r_p\right) - r_p \right] \tag{4.14}$$

$$F = \frac{\mu_0 J_c^{\,2}}{4\pi} \frac{1}{\left(r_a - r_p\right)} \left[ r_a - r_p \ln\left(r_a\right) - r_p \ln\left(r_p\right) - r_p \right] \tag{4.15}$$

Equation (4.15) is quite a bit larger in magnitude compared to the tip term from the MPD equations, and the pinch term still hasn't been computed. The large magnetic fields at the end of the anode cause the large differences in the force being produced at the end of the center electrode from the two machines.

The pressure term during the collapse has a similar result to that of the rundown. The second integral from equation (4.8) is zero because it has the same magnetic field dependence as the rundown phase. The velocity of the plasma sheath during the collapse phase is roughly constant, which makes the first integral zero. So the force term that results from the pressure is equation (4.16).

$$F = \frac{1}{\left(r_a - r_p\right)} p(r_0, z) \pi \left[ \frac{2 r_a^{\,3}}{3} - r_p r_a^{\,2} - \frac{r_p^{\,3}}{3} \right] \tag{4.16}$$

The force in equation (4.16) is dependent on the average area during the collapse, and results from integrating the differential area using the same limits as equation (4.12). Using the same arguments that were presented in the rundown phase, this term should be negligible.

### 3. Pinch

The pinch force has to be analyzed a little bit differently than the rundown and collapse phases. The plasma in the pinch region might carry some current, but very little of the current will be in the radial direction. Since a small amount of current is moving in the radial direction, the $\vec{J} \times \vec{B}$ force in the z direction will be negligible, leaving only the pressure term to apply a force. The gas dynamic pressure will be the only pressure acting, like in the rundown and collapse phases. The gas dynamic pressure can be found using equation (4.17), which is the Bennett Pinch relation.

$$P = nkT \tag{4.17}$$

where n is the particle density and kT is the plasma temperature. Multiplying equation (4.17) by the area and converting to the linear particle density results in equation (4.18).

$$F = \frac{NkT}{\pi r_p^{\,2}} \pi r_p^{\,2} \tag{4.18}$$

Accounting for the fact that volume is area multiplied by length, equation (4.18) can be simplified to equation (4.19).

$$F = NkT \tag{4.19}$$

Experimental values are needed to solve equation (4.19). Typical values for the TAMU DPF are 6 keV for the plasma temperature, pinch radius of 1 mm, pinch length of 1 cm, and a particle density of 1E21 particles per cubic centimeter. With those values, the force results in approximately 60,000,000 dynes which is roughly 600 N. This is a simplified model of the pinch and does not take into account any nonlinear effects.

## B. Thrust Calculated from Working Data

This section will calculate the thrust generated by the TAMU DPF. The force for each phase of motion will be computed using the known values for the change in velocity, time and estimated mass in each phase. The velocities produced by the thrust models will then be compared to the experimentally know velocities. Equation (4.20) shows the governing equation for this method.

$$F\Delta t = m\Delta v \tag{4.20}$$

Equation (4.20) is simply an alternate form of Newton's second law. Table 4.1 gives the working parameters for the TAMU DPF, which will be used to help verify the equations modeling the DPF. These values are for an initial gas fill pressure of 10 torr, and deuterium as the fuel.

**Table 4.1 Working Parameters for the TAMU DPF**

| Phase | Ion Energy at End of Phase [eV] | Final Velocity [m/s] | Mass [kg] | $\Delta$t [s] |
|---|---|---|---|---|
| Rundown | ~60 | 53,500 | 4.52E-06 | 3.80E-06 |
| Collapse | ~600 | 169,000 | 3.18E-07 | 3.00E-07 |
| Pinch | ~70000 | 1,830,000 | 8.84E-09 | 1.00E-07 |

The mass for the rundown phase is approximated by assuming that only the initial gas in the rundown region will be picked up by the sheath. It is known that a portion of the gas in not ionized and escapes through the outer electrode, so the total mass (static fill mass within the rundown region) is multiplied by eight tenths to estimate the actual mass. The mass for the collapse phase is calculated from the gas that is present under the anode radius and then between the end of the anode and 0.02 m from of the end of the anode. Following the estimation by Mather, 10% of mass from the collapse region is assumed to be compressed into the pinch region[9]. The data in Table 4.1 reflects these assumptions.

To be able to use the values presented in Table 4.1 to estimate the thrust, more input data from the TAMU DPF are needed. Table 4.2 gives the input current, radii and lengths required to complete the force calculations. The anode length listed has been adjusted to the length where thrust will be produced, i.e. the length from the end of the insulator to the end of the anode.

**Table 4.2 Dimensions and Max Current for TAMU DPF**

| Max Current [MA] | Anode Radius [m] | Cathode Radius [m] | Plasma Radius [m] | Anode Length* [m] |
|---|---|---|---|---|
| 1.4 | 0.0508 | 0.0762 | 0.001 | 0.2032 |

Using the data presented in Table 4.2 and equations (4.6), (4.9), (4.15), (4.16), and (4.19) the force for each phase of motion can readily be calculated. Using the force for each phase, Table 4.1 and equation (4.20), the velocities at the end of each phase of motion can be computed. The plasma energy at the end of each phase can then be computed using the non relativistic kinetic energy equation. All of these values are

presented in Table 4.3. All of the gasdynamic pressure values are approximated to be zero in Table 4.3. The current during the collapse and the pinch is approximated to be 80% of the maximum current, because of the change of inductance during the plasma motion.

**Table 4.3 Calculated Forces and Velocities**

| Phase | Force [N] | Velocity [m/s] | Ion Energy [eV] |
|---|---|---|---|
| Rundown | 79,500 | 6.68E+04 | 90 |
| Collapse | 150,000 | 1.41E+05 | 400 |
| Pinch | 600 | 6.79E+03 | 1 |
| Total Force | 230,000 | | |

Theoretically the collapse and the pinch produce the highest thrust for the DPF. Using the data in Table 4.1 and equation (4.20), the force for each phase of motion for the TAMU DPF was evaluated and the results are presented in Table 4.4. The collapse term is broken up into the r and z components, and is listed as such in Table 4.4. The pinch terms was calculated by approximating the non fusion ions to have an ion energy of 100 keV after the pinch.

**Table 4.4 Actual TAMU DPF Forces, and Velocities**

| Phase | $\Delta$t [s] | m [kg] | $\Delta$v [m/s] | F [N] | Energy [eV] |
|---|---|---|---|---|---|
| Rundown | 3.80E-06 | 4.52E-06 | 5.35E+04 | 64,000 | 60 |
| Collapse | 3.00E-07 | 3.18E-07 | 1.69E+05 | 180,000 | 597 |
| z | | | 1.66E+04 | 18,000 | 6 |
| r | | | 1.69E+05 | 179,000 | 592 |
| Pinch | 1.00E-07 | 8.84E-09 | 1.79E+06 | 162,000 | 70,000 |
| Total | 4.20E-06 | 4.85E-06 | | 244,000 | |

A comparison between Table 4.3 and Table 4.4 shows that the plasma velocities are less in each phase for the TAMU DPF. The energies listed in Table 4.4 are the computed ion energies at that the end of the phase of motion, assuming all ions will be at the calculated velocity. It should be noted that velocity prior to the plasma sheath reaching each phase of motion is zero. The total thrust listed in Table 4.4 is the combination of the rundown, z component of the collapse, and the pinch. The total thrust is the thrust produced for each time the DPF is fired, with the thrust being applied over the $\Delta t$ plus the ~1 $\mu s$ where the plasma sheath is in the inverse pinch phase. The experimental data suggests that the TAMU DPF produces a slightly higher thrust than is predicted by the theoretical model.

The collapse phase had a considerable difference in force between the theoretical model and the experimental data. This difference will be attributed to the fact that the experimentally the plasma sheath does not resemble the model used. Referring to Figure 2.4, it can be seen that there are considerable differences between the idealized plasma sheath collapse and the actual plasma sheath collapse.

To investigate the dependence upon the assumption that plasma collapses to half a centimeter off the end of the anode, Table 4.5 was made. Table 4.5 shows how the thrust varies for this case, along with also determining the specific impulse and efficiencies. The specific impulse and efficiencies were calculated using equation 2.3 and 2.4. For these calculations the totals listed in Table 4.4 were used. The bank energy used for the calculation is the energy that the TAMU DPF charges to for normal operation, 120 kJ.

**Table 4.5 Collapse Distance Effect on TAMU DPF Performance**

| Zcollapse [m] | 0.002 | 0.003 | 0.004 | 0.005 | 0.006 | 0.007 | 0.008 |
|---|---|---|---|---|---|---|---|
| Force [N] | 233,000 | 236,000 | 240,000 | 243,000 | 247,000 | 250,000 | 253,000 |
| Isp[s] | 6,300 | 6,400 | 6,500 | 6,600 | 6,700 | 6,800 | 6,900 |
| Eff | 82% | 85% | 87% | 89% | 92% | 95% | 97% |

As can be seen in Table 4.5, the TAMU DPF will produce a force greater than 243,000 N with a specific impulse of greater than 6,600 s, with an efficiency of roughly 89%. The chart shows all three performance indicators increase as the collapse distance from the end of the anode increases.

## C. Duty Cycle

Duty cycle is a term that applies to pulsed thrusters. It simply refers to how often the thruster needs to be pulsed. The lower the duty cycle is that is required, means the fewer times the thruster needs to be pulsed. An attainable duty cycle is critical for the DPF as a thruster because the thrust occurs of such short time intervals.

A simple analysis that can be done to determine what type of duty cycle is need, is to determine the time averaged thrust. This entails integrating the thrust over the time the thrust is applied, and dividing by one second. To surpass the MPD in time average thrust, the DPF will have to pulse the thruster numerous times compared to the MPD. The number of pulse with the DPF per pulse of the MPD that results in approximately the same time averaged thrust is 75. The time average thrust for the DPF is given by equation (4.21).

$$T_{time\ averaged} = NT_{per\ pulse}\Delta t \tag{4.21}$$

N is the number of shots. The MPD thrust at 1.4 MA is 80,000 N, and the time the force is applied over is one millisecond. This comparison was made using the TAMU DPF data and the theoretical data for the MPD.

**D. Erosion**

Erosion of the electrodes is one of the biggest drawbacks to using a coaxial plasma thruster. This case certainly is no different for the DPF. The erosion of the DPF is markedly different that than of the MPD, whereas, all of the erosion occurs along the electrode axis at the tip of the anode. Very little ablation occurs anywhere else in the system because of the short amount of time that the plasma actually spends at a given location. Figure 4.3 shows what the end of an anode's hole is supposed to look like originally.

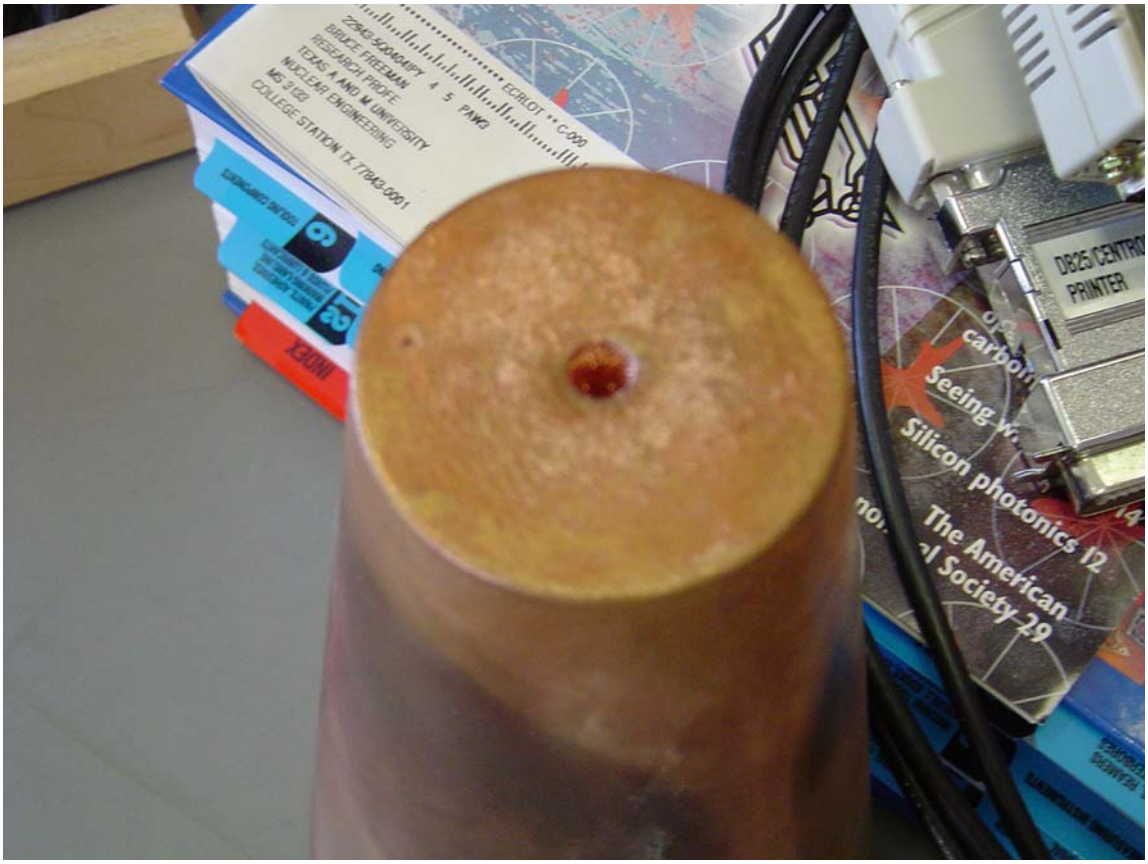


**Figure 4.3 Original End of the Anode Hole for TAMU DPF**

Figure 4.4 shows a picture of what the erosion looks like on the anode of the TAMU DPF. These pictures are a little misleading since they are not the same anode. What it is supposed to show is that the anode originally has a small hole, and then develops a much larger hole after being used for numerous shots.

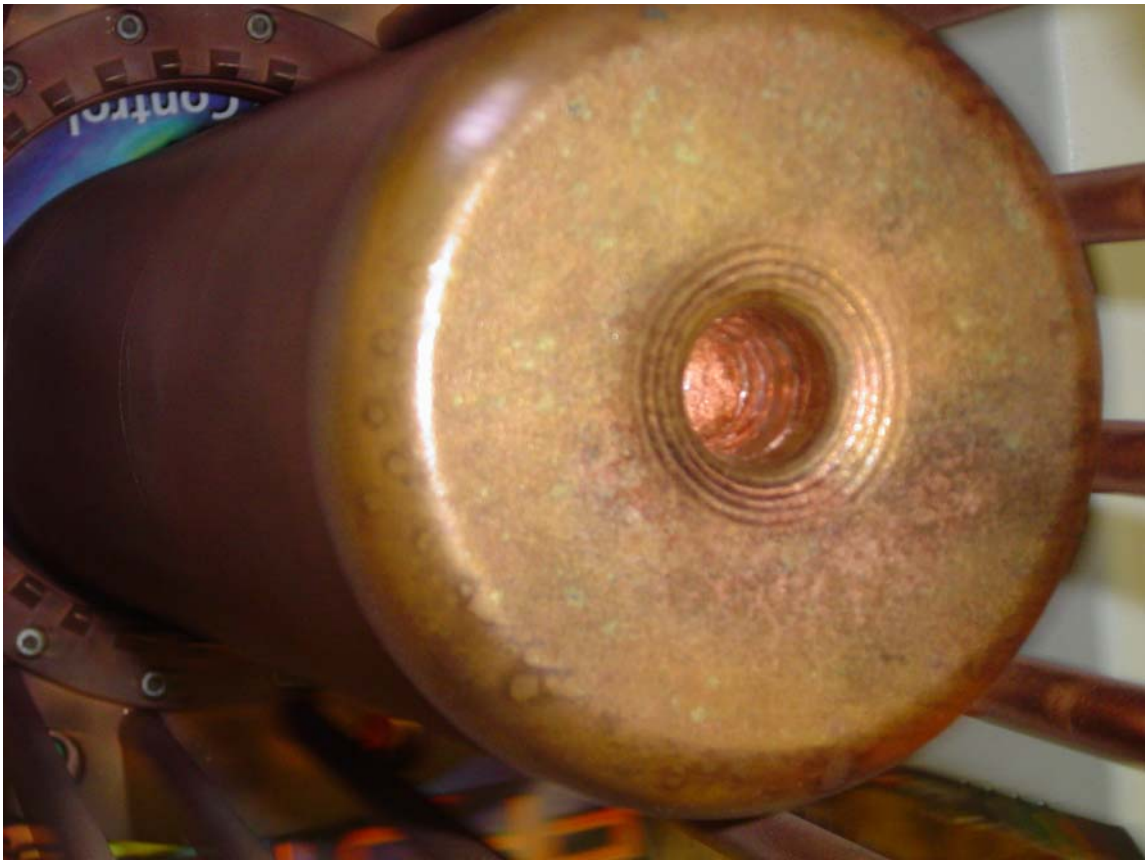

**Figure 4.4 End of the Anode Erosion for the TAMU DPF**

# CHAPTER V

# CONCLUSIONS AND RECOMMENDATIONS

The thrust models developed show that there is some agreement between the experimental data and the theoretical computations. The models show that for the DPF to be feasible for long term space missions it will be heavily dependent on the duty cycle. The DPF should produce a larger force than the MPD for similar input current and geometry, but the DPF applies the force over a much shorter period of time. The pulse from the DPF does not last long enough for the DPF to compete with the MPD unless a rapid firing capability can be developed. Without a rapid firing capability, the DPF fusion potential will need to be developed if the DPF is to be considered for future space missions.

The experimental data for the TAMU DPF and the force dependence on current from the theoretical models show that the values predicted in previous research efforts are low. The thrust produced by the TAMU DPF is roughly half of the force that was predicted by the group from Purdue, and uses one twentieth of the input current. Since force scales as the current squared, the force values should be roughly 400 times greater than values computed using the TAMU DPF experimental data. Also, the mass flow rate values used in the Purdue effort are much higher than is calculated from the TAMU DPF experimental data.

There are a few areas that still need to be addressed. The validity of the equations will remain unproven until experiment thrust measurements are made. More specifically, thrust measurements will need to be made that can separately measure the collapse and

pinch term. Separating the rundown force from the collapse and pinch force can be done by making ballistic pendulum thrust measurements at the end of the anode, instead of downstream of the electrode system. Also, the collapse term should undergo a more realistic computation to provide a more accurate thrust value. Future modeling will need to take into account the shape of the plasma sheath as it collapses toward the axis. Finally, erosion studies will need to be conducted on the DPF to determine its feasibility for deep space missions. Since the erosion from the DPF occurs on the electrode axis, it might be possible to design a separate center section that is designed to replace the material that is eroded away. This could possibly be accomplished by using a removable insert at the center of the anode which would allow the eroded piece to be removed and replaced, with minimal loss of operation time. Pipe electrodes should also be studied to see if they provide any erosion benefits.

# REFERENCES

[1]Garwin, R., Rosenbluth, A., Rosenbluth, M. “Infinite Conductivity Theory of the Pinch.” Los Alamos Scientific Laboratory Report, Los Alamos, NM, 1955.

[2]Choi, C., Cox, L. “Engineering Considerations for the Self-Energizing Magnetoplasmadynamic (MPD) – Type Fusion Plasma Thruster”. Phillips Laboratory Report. Edwards AFB, CA, 1994.

[3]Nardi, V., Powell, C., Brozosko, J. S. “Evaluation of the Plasma Focus as a Thruster with Neutron-Lean Fusion Reactions”. Phillips Laboratory Report, Edwards AFB, CA, 1993.

[4]Miley, G.H., Javedani, J.B., Temple, B.A., Kislev, H., Nachtrieb, R.T. “Flowing DPF Design for Propulsion Experiments”. Phillips Laboratory Report, Edwards AFB, CA, 1993.

[5]Miley, G.H., Nadler, J., Temple, B.A., Bolt, S., Kislev, H. “Critical Technology Demonstration of Plasma Focus Type MPD Thrusters”. Phillips Laboratory Report, Edwards AFB, CA, 1992.

[6]Maecker, H. “Plasma Jets in Arcs in a Process of Self-induced Magnetic Compression,” *Zeitschrift fur Physik*, Vol. 141, No. 1, 1955

[7]Jahn, R.G., *Physics of Electric Propulsion*, McGraw-Hill, New York, 1968.

[8]Rudolph, L.K., “The MPD Thruster Onset Current Performance Limitation”, Ph.D. Dissertation, Princeton University MAE Dept, Princeton, NJ, 1980.

[9]Mather, J.W., “Dense Plasma Focus”, *Methods of Experimental Physics Vol. 9B*, edited by H Lovberg and H R Griem, Academic Press, New York, pages 187-249, 1971.

# VITA

Richard Lee Hardy holds a B.S. degree from Texas A&M University in Aerospace Engineering with a minor in Nuclear Engineering. This thesis was written to fulfill graduation requirements for a M.S. in Nuclear Engineering from Texas A&M University. Richard Lee Hardy's permanent address is 18114 Veranda Lane, San Antonio, Texas 78258.